Preparation and Photophysical Properties of *o*-Carboranyl AIEgens Containing Regioisomeric N-Phenyl-Carbazole*

JIN Xiaoping, WU Xueyan, LYU Yan, GUO Jixi†

(*State Key Laboratory of Chemistry and Utilization of Carbon Based Energy Resources, Key Laboratory of Advanced Functional Materials, Xinjiang Uygur Autonomous Region of China, Institute of Applied Chemistry, School of Chemistry, Xinjiang University, Urumqi Xinjiang 830017, China*)

Abstract: This work described here a new design strategy for obtaining *o*-carboranyl compounds containing regioisomeric N-phenyl-carbazole with AIE properties. Two *o*-carborane functionalized N-phenyl-carbazole compounds (C3DC and C9DC) were synthesised and fully characterised. Photoluminescence experiments confirmed both compounds have strong AIE activity. The two *o*-carborane-functionalised N-phenyl-carbazole isomers have high solid-state fluorescence quantum yields, reaching 99% and 93%, respectively. In addition, based on the results of DFT calculation, the emission bands could be attributable to ICT transitions from N-phenyl-carbazolemoieties to the *o*-carborane units.

Key words: *o*-carborane; N-phenyl-carbazole; regioisomeric; aggregation-induced emission; intramolecular charge transfer
DOI: 10.13568/j.cnki.651094.651316.2021.09.28.0001
CLC number: O436 **Document Code:** A **Article ID:** 2096-7675(2022)04-0446-09
引文格式: 靳小平, 吴雪岩, 吕燕, 郭继玺. 聚集诱导发光邻碳硼烷-咔唑区位异构体的合成及光物理性质研究[J]. 新疆大学学报(自然科学版)(中英文), 2022, 39(4): 446-454.
英文引文格式: JIN Xiaoping, WU Xueyan, LYU Yan, GUO Jixi. Preparation and photophysical properties of *o*-carboranyl AIEgens containing regioisomeric N-phenyl-carbazole[J]. Journal of Xinjiang University(Natural Science Edition in Chinese and English), 2022, 39(4): 446-454.

聚集诱导发光邻碳硼烷-咔唑区位异构体的合成及光物理性质研究

靳小平，吴雪岩，吕 燕，郭继玺

(新疆大学 化学学院，应用化学研究所，省部共建碳基能源资源化学与利用国家重点实验室，
先进功能材料自治区重点实验室，新疆 乌鲁木齐 830017)

摘 要： 通过简单的合成策略制备出具有聚集诱导发光性质的邻碳硼烷-N-苯基咔唑区位异构体化合物（C3DC和C9DC），并对其结构进行了表征. 两种化合物均具有聚集诱导发光性质，固态下化合物C3DC和C9DC的发光量子产率分别高达99%和93%. DFT理论计算结果表明，化合物的发光主要源于分子内邻碳硼烷与咔唑之间产生的分子内电荷转移.

关键词： 邻碳硼烷；N-苯基咔唑；区位异构体；聚集诱导发光；分子内电荷转移

0 Introduction

Solid-state luminescent materials, which pose excellent photoluminescence (PL) quantum yields, higher electroluminescence efficiencies and small efficiency roll-off are becoming hot topics of current research worldwide[1]. The efficient solid-state luminescent materials are relatively insufficient because the usual design strategy of it is to introduce and extend aryl or heteroaryl groups to broaden π-conjugation and have a red-shift of the spectra. However, the usual design strategy oft-

* **Received Date:** 2021-09-28
Foundation Item: National Science Foundation of China(U2003307; 21861037); Opening Project of Xinjiang Key Laboratory(2017D04014); Natural Science Foundation of Xinjiang Uygur Autonomous Region of China(2020D01C062); Scientific Research Program of the Higher Education Institution of Xinjiang(XJEDU2021Y005); Xinjiang Tianchi Doctoral Project(tcbs201934); Xinjiang University Doctoral Research Foundation(BS190227); Research Innovation Project of Postgraduate students in Autonomous Region(XJ2020G038).

Biography: JIN Xiaoping (1994-), female, master, research fields: aggregation-induced emission (AIE) materials.
† **Corresponding author:** GUO Jixi (1979-), professor, research fields: photochemistry and carbon functional materials, E-mail: jxguo1012@163.com.

en causes aggregation-caused quenching (ACQ) which left lots of troublesomes for their application. In 2001, Tang and his co-workers proposed the concept of AIE, which emphasize that the materials significantly promoted bright luminescence in the aggregate or solid state[2]. Therefore, many researchers have always centered on the development of novel efficient solid-state luminescent materials, among which the *o*-carborane containing derivatives are a kind of efficient materials exhibiting great potential in solid-state luminescent materials emission.

o-Carborane, an icosahedralboron-cluster via the three-center two-electron bonds, with high thermal and electrochemical stabilities has been extensively applied in boron neutron capture therapy (BNCT)[3], OLEDs[4], chemical sensing[5], and optical functional materials[6] in recent years. *o*-Carborane considered as a three-dimensional (3D) variant of benzene shows great electron-withdrawing ability which is in favor of design of D-A (D=donor, A=acceptor) conjugated materials which exhibit intriguing luminescent features due to the intramolecular charge transfer (ICT) process[7−9]. Indeed, *o*-carboranes appending to various electron donors such as naphthyl[10], anthracenyl[11], tetraphenyl ethenyl[12], pyrenyl[13] chrysenyl[14], and carbazolyl[15] groups exhibit multiple photoluminescence emissions features, such as aggregation-induced enhanced emission (AIEE), crystallization-induced emission enhancement (CIEE), thermally activated delayed fluorescence (TADF), aggregation-induced delayed fluorescence (AIDF) and so on, which triggered by twisted intramolecular charge transfer (TICT) states. Furthermore, our group has reported a series of aryl or heteroaryl groups have been applied to electron donors in D-A dyads/triads to enhance the ICT transition due to their electron-rich features[13,15−16]. Among them, *o*-carborane functionalized carbazole compounds have attracted significant attention due to their unusual multiple photoluminescence properties that derive from their structural rigidity. However, *o*-carborane functionalized carbazole compounds vary considerably in the photophysical behavior by altering the electronic environment of the carbon atoms of the carbazole moiety in such D-A triads, which rarely been investigated.

To insight into the detailed relationships between molecular structure and photophysical properties of *o*-carborane functionalized carbazole compounds, particularly the effect of the substitution position of the *o*-carborane in carbazole on the emissive character via ICT transitions, we herein design synthesis and photophysical properties of two *o*-carborane functionalized N-phenyl-carbazole compounds (C3DC and C9DC) in which regioisomeric N-phenyl-carbazole were introduced to the *o*-carboranes, respectively. This enabled us to elucidate the impact of the *o*-carborane substitution position on photophysical properties involving ICT transitions. The photoluminescent properties of the *o*-carborane functionalized carbazole compounds were studied with steady-state UV-Vis absorption fluorescence spectra and DFT calculation.

1 Experimental Section

1.1 General Procedures

All reactions were carried out under a dry N_2 atmosphere. Solvents of THF and toluene were distilled from sodium/benzo -phenone and stored over molecular sieves. Other chemicals were purchased from Energy and Aladdin chemical reagent company and used without further purification. All reactions were monitored by thin layer chromatography (TLC). Column chromatography was conducted using silica gel (300~400 mesh).

1.2 Analytical Measurements

NMR spectra were recorded on a Bruker ADVANCE III 400 MHz spectrometer (^{1}H NMR: 400 MHz, ^{13}C NMR: 100 MHz). All chemical shifts were reported in δ units with references to the residual solvent resonances of the deuterated solvents for proton and carbon chemical shifts. Mass spectra were obtained on an Ultimate 3000/Q-Exactive spectrometer. Melting points were measured using a Nikon Polarizing Microscope ECLIPSE 50i POL equipped with an INTEC HCS302 heating stage. UV-Vis absorption spectra were recorded on a Hitachi U-3900H. Fluorescence spectra were performed on Horiba FluoroLog-3 spectrofluorometer (Horiba–Jobin–Yvon, Edison, NJ, USA). Luminescence lifetime measurements were carried out by using a FluoroLog-3 spectrofluorometer, absolute PL quantum yield (Φ_{PL}) was determined using a Horiba FL-3018 Integrating Sphere. The temperature dependent luminescence spectra were measured with Janis VPF-100 liquid nitrogen low temperature thermostat (Janis, USA).

1.3 DFT Calculation

The optimized structures and frontier orbitals (HOMO: highest occupied molecular orbital; LUMO: lowest unoccupied molecular orbital) were calculated by using density functional theory (DFT) and time-dependent DFT (TD-DFT) at the

B3LYP/6-31 G (d, p) level by using the Gaussian 09 suite of programs in the ground and excited states. Structure optimization was performed before the calculation of the HOMO/LUMO energies[15,17].

1.4 Synthesis

1.4.1 Synthesis of C3DC

To a THF solution (10 mL) of *o*-carborane (288 mg, 2.0 mmol) was slowly added ^{i}PrMgCl (2.0 M in THF, 2.4 mL, 4.8 mmol) at 0 ℃ under N_2 atmosphere for 3 h, and the mixture was stirred at room temperature for 10 h. After replacement of THF with toluene (10 mL), addition of 3-bromo-9-phenylcarbazole (1.55 g, 4.8 mmol, 2.4 equiv) and $NiCl_2$ (46 mg, 0.2 mmol), the reaction mixture was heated at 115 ℃ under stirring for 12 h in a closed flask. Then, the reaction was quenched with water (10 mL) and the organic layer was extracted with CH_2Cl_2 (3×30 mL) and dried over $MgSO_4$. The solvent was removed under reduced pressure and the residue was purified by silica gel column chromatography using DCM/petroleum ether (1/6, v/v) as the eluent to obtain pale yellow compounds C3DC (526 mg, 63%). Mp: 182.6~184.1 oC, 1HNMR (400 MHz, $CDCl_3$): δ 8.32 (d, J= 4.0 Hz, 2 H), 8.09 (t, J = 4.0 Hz, 1 H), 8.07 (t, J = 4.0 Hz, 1 H), 7.56~7.50 (m, 6 H), 7.43~7.39 (m, 2 H), 7.38~7.34 (m, 6 H), 7.29~7.24 (m, 4 H), 7.09 (d, J = 8.0 Hz, 2 H), 3.15~1.60 (10 H, br, B–H). ^{13}C NMR (100 MHz, $CDCl_3$): δ 141.93, 141.24, 136.79, 129.83, 128.39, 127.76, 126.84, 126.57, 123.37, 123.02, 1 222.78, 120.44, 120.35, 109.99, 109.20, 88.01. HRMS: m/z calcd for $C_{38}H_{34}B_{10}N_2[M]^-$: 626.371 97，Found: 626.374 51.

1.4.2 Synthesis of C9DC

This compound was prepared in a manner analogous to the synthesis of C3DC using 9-(4-bromophenyl)-carbazole (1.55 g, 4.8 mmol, 2.4 equiv) to replace 3-bromo-9-phenylcarbazole to give acolorless powder of C9DC (788 mg, 63%.). Mp: >250 ℃ 1HNMR (400 MHz, $CDCl_3$): δ 8.11 (t, J= 4.0 Hz, 2 H), 8.09 (t, J = 4.0 Hz, 2 H), 7.75 (d, J= 8.0 Hz, 4 H), 7.48 (d, J= 8.0 Hz, 4 H), 7.28~7.19 (m, 12 H), 3.50~1.60 (10H, br, B–H). ^{13}C NMR (100 MHz, $CDCl_3$): δ 141.71, 141.18, 136.89, 130.05, 128.02, 126.97, 125.52, 124.93, 123.29, 122.58, 120.68, 120.41, 120.01, 110.19, 109.75, 77.97, 61.33. HRMS: m/z calcd for $C_{38}H_{34}B_{10}N_2[M]^-$: 626.371 97，Found: 626.378 36.

2 Results and Discussion

2.1 Design and Synthesis of the Compounds

Carbazole has been one of the most important and thoroughly investigated organic chromophore in previous years due to their high thermal and photochemical stability, pure blue fluorescence, planar geometry and natural high charge carrier mobility[18]. In addition, the carbazole is a strong electron donor, with a large Stokes shift, long excited lifetime and considerable chemical stability, making them valuable members of a panel of conventional fluorophores *o*-carborane was selected to tune the excited state of organic chromophores. Two regioisomeric N-phenyl-carbazole were introduced to the carbon atoms of the *o*-carborane to synthesize C3DC and C9DC via a modified nickel-catalyzed cross-coupling reaction indifferent reactive sites (Fig 1)[13,15−16,19]. All compounds were obtained with moderate to satisfactory yields and the products exhibited fine stability under ambient conditions and stability high enough for spectroscopic measurements. The molecular structures were fully verified with NMR and HRMS spectra.

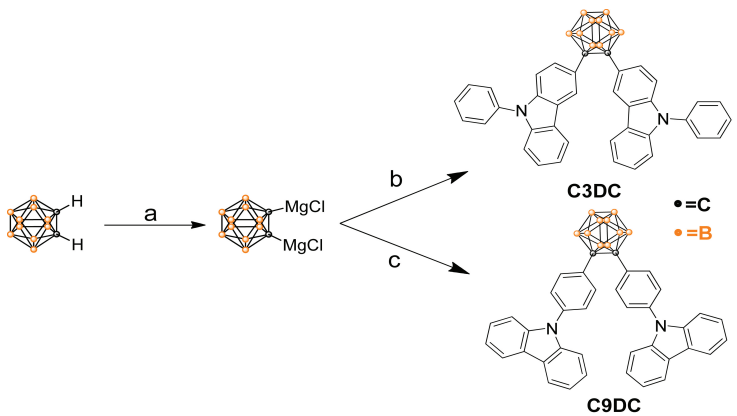

Fig 1 (a) THF, 1.2 eq *i*PrMgCl, 0 ℃ for 3 h, room temperature for 10 h; (b) Toluene, 2.4 eq 3-bromo-9-phenyl carbazole, $NiCl_2$, 115 ℃, 12 h. (c) Toluene, 2.4 eq 9-(4-bromophenyl)-carbazole, $NiCl_2$, 115 ℃, 12 h

2.2 Steady-State Electronic Spectroscopy(UV-Vis absorption and emission spectra)

The UV-Vis absorption spectra of C3DC and C9DC were studied. As shown in Fig 2 and Table 1, UV-Vis absorption spectra of C3DC and C9DC were measured in different solvents. *o*-Carborane as an electron withdrawing unit in C3DC and C9DC does not show any significant absorption in the absorption spectra. The absorption bands in the region of 320 nm~360 nm in C3DC and C9DC were assigned to the π-π^* transitions on the carbazole groups, and no significant electronic coupling between carbazole and *o*-carborane moiety in the ground state[20] Solvent dependency studyof UV-Vis absorption spectra for C3DC and C9DC hardly observed, further indicating that the ground state was not affected by the solvent polarity.

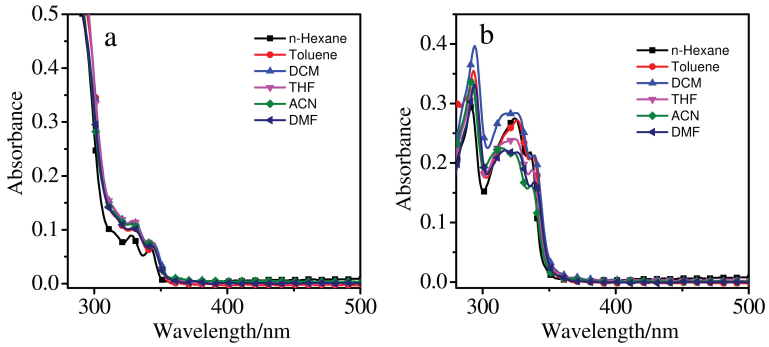

Fig 2 UV-Vis absorption spectra of (a) C3DC and (b) C9DC in different solvents, c=1.0×10^{-5} M, 20 ℃

Table 1 Photophysical properties of C3DC and C9DC

Samples	λ_{abs}/nm	λ_{em}/nm	τ_F/ns	Φ_F/%
C3DC	278, 329, 344	-^{a,f}, 550^b, 530^c, 548^d	2.91^a, 9.81^b, 6.58^c, 7.77^d	-^{a,f}, 56.8^b, 99^c, 99^d
C9DC	292, 324, 337	375^a, 556^b, 545^c, 556^d	5.41^a, 20.01^b, 14.18^c, 13.88^d	-^{a,f}, 34.7^b, 93.19^c, 86.1^d

Note: *a*: Measured in THF solution (1×10^{-5} M) at room temperature; *b*: f_W=99%; *c*: In the solid state; *d*: In neat film; *e*: For lifetimes monitored at different wavelengths; *f*: Not detected.

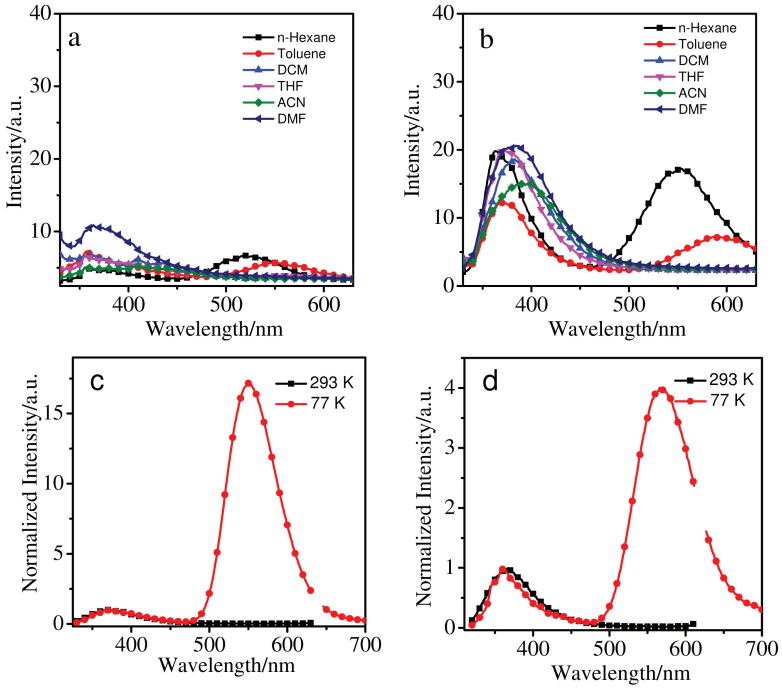

Fig 3 The emission spectra of (a) C3DC (b) C9DC in different solvents, and (c) C3DC, (d) C9DC in 2-MeTHF solution at room temperature (black line) and at 77 K (red line), λ_{ex}=330 nm, c=1.0×10^{-5} M, 20 ℃

To elaborate the emission mechanism of C3DC and C9DC, optical spectra in various solvents were measured (Fig 3 and Table 1). The C9DC exhibited dual-emissive property in the solution (Fig 3b). Sharp emission bands with vibrational structures and broad ones were observed with peaks at around 370 nm and 550 nm, respectively, which indicated that the emission bands of C9DC around 370 nm and 550 nm are from the locally excited (LE) and ICT states[15−16,21]. However, for C3DC, the emission intensity is too low to measure (Fig 3a). Moreover, we measured the emission spectra at low temperature of 77 K in 2-MeTHF solution where the molecular motions are completely suppressed (Fig 3c and 3d). In contrast to these characters from emission at room temperature in 2-MeTHF, C3DC and C9DC showed strong broad emission in the longer-wavelength region, but the short wavelength emission bands with vibration structures is similar to that at room temperature. The above results revealed that the substitution position of the *o*-carborane in carbazole have effect on the emissive character via ICT transitions.

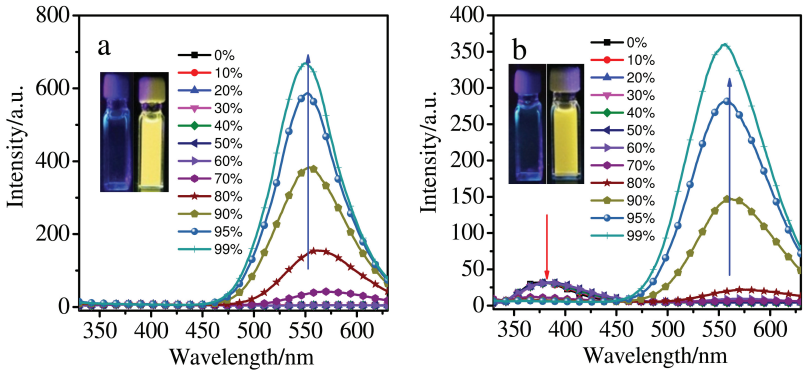

Fig 4 Fluorescence spectra of (a) C3DC and (b) C9DC in THF/water mixtures with different water volume fractions, λ_{ex}=330 nm, c=4.0×10^{-5} M, 20 ℃. Inset: photographs taken under UV illumination in the different water fractions

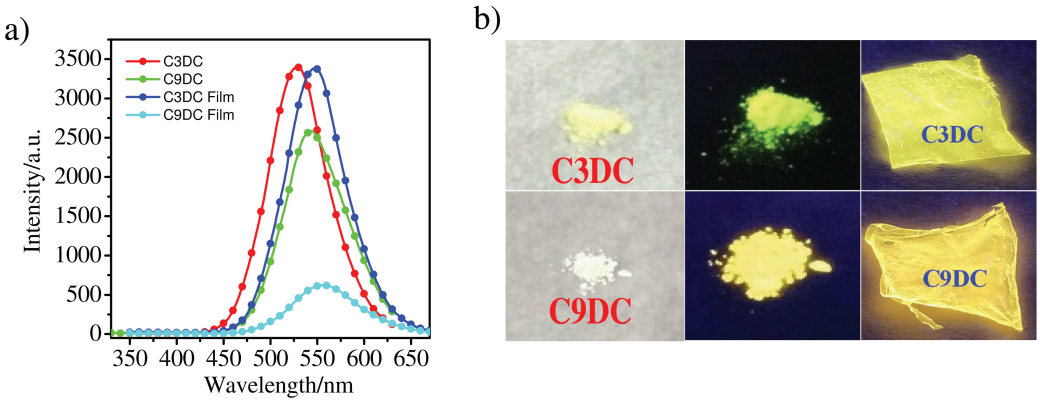

Fig 5 (a) Emission spectra of C3DC and C9DC in different states (b) Photographs of compounds C3DC and C9DC as solid powders under day light (left), fluorescent images under UV illumination (365 nm, middle) and photographs of compounds C3DC and C9DC in 5% PMMA neat film under UV light illumination (365 nm, right)

Next, the aggregation and solid-state emission properties of C3DC and C9DC were estimated (Fig 4 and Table 1). Thanks to the introduction of regioisomeric N-phenyl-carbazole into two carbon atoms of optically functional "element-block" *o*-carborane in different reactive sites, C3DC and C9DC showed typical AIE characteristic. The AIE characteristic of C3DC and C9DC was further proved by studying their PL behaviors in THF and THF/water mixtures with different water fractions (f_w)(Fig 4 and Table 1). In dilute THF solution, C3DC and C9DC were weakly emissive owing to the vibrations of C_{cage}–C_{cage} bond in *o*-carborane which quenched the emission in solution[22]. With the increase of water in THF solutions results in the formation of insoluble aggregates which can enhance the emission of compounds. The highest emission was achieved at f_w=99%. The quantum yields of C3DC and C9DC in dilute THF solutions were determined to be less than 0.1% by a calibrated integrating sphere. In the aggregated state, their quantum yields were measured to be 56.8% and 34.7%. Correspondingly, an intense broad emission band around 548 nm and 556 nm was obtained for C3DC and C9DC, respectively,

and with bright yellow emission under the 365 nm UV light irradiation (Fig 4 insert). However, accompanying the increase in the water content, blue-shifted emission bands were observed in Fig 4, which attributed to the molecules aggregate into nanoparticles, whose polarity inside is lower than that outside. And the emission bands are blue-shift similarly to typical ICT emission[15]. The above results indicate that C3DC and C9DC are all AIEgens.

The emission properties in the solid and film states were examined (Fig 5 and Table 1). From the emission spectra in the solid state and in film state, the C3DC and C9DC were pale yellow and white under daylight illumination. In Fig 5a, the solid-state emission peaks of C3DC and C9DC are 530 nm and 545 nm, respectively, and the emission peaks are shifted by 15 nm. As depicted in Fig 5b, under 365 nm UV light irradiation, strong yellow emissions for C9DC, bright yellow green emission for C3DC were observed from the solid and film state under 365 nm UV light irradiation. The absolute emission quantum yields for C3DC and C9DC in the solid state and film state were also evaluated (Table 1). Interestingly, the emission efficiency with QY up to 99% and 93.7% were achieved for C3DC and C9DC, respectively. This fact strongly suggests that the emission band in the solid-state should be induced by the ICT state and the reactive sites play an important role in manipulating the degree of ICT process.

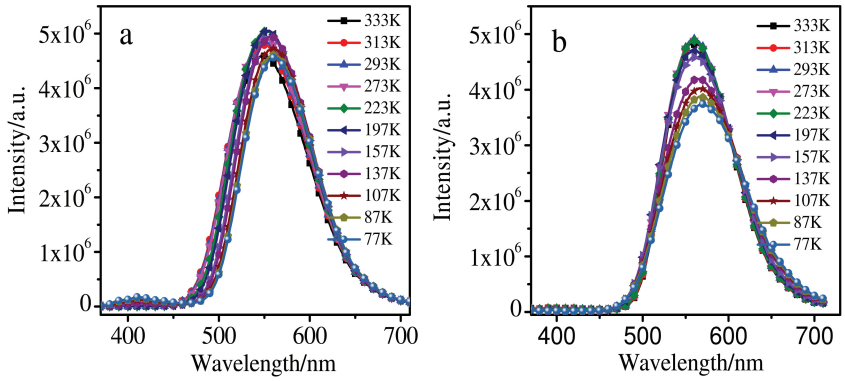

Fig 6 The emission spectra of (a) C3DC and (b) C9DC in the solid state during heating from 77 K to 333 K

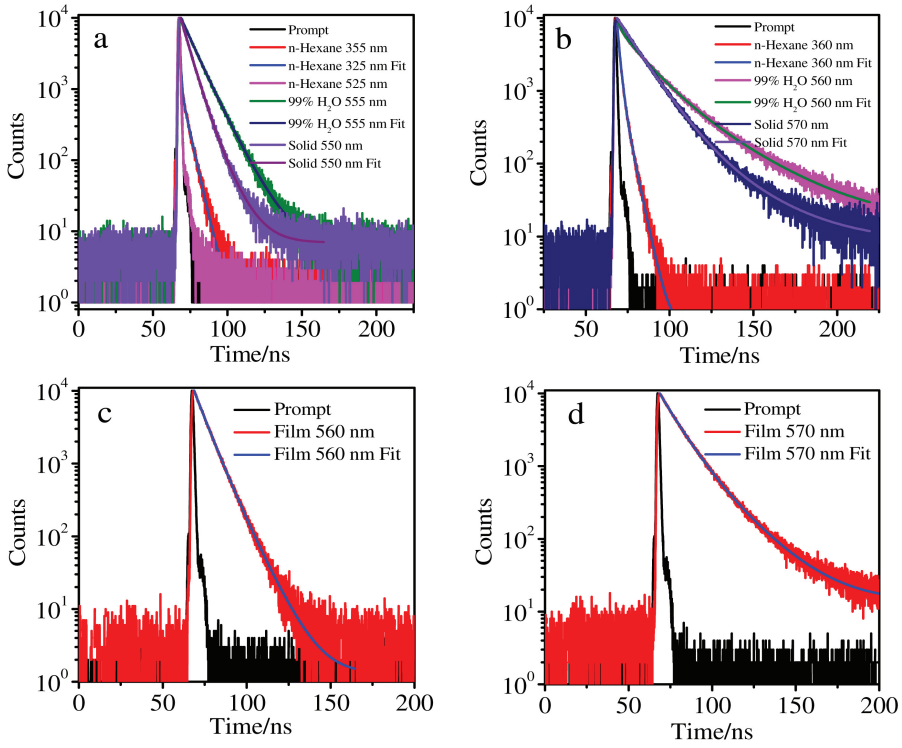

Fig 7 Emission decay profiles for (a), (c) C3DC and (b), (d) C9DC in different states

Thermochromic behavior in luminescence from C3DC and C9DC were investigated with the powder samples (Fig 6). In order to avoid the powder samples decomposing when heated, we evaluated the thermochromic luminescence properties below melting point. Emission spectra were monitored on the liquid nitrogen low temperature thermostat by increasing the temperature from 77 K to 333 K (before melting). The C3DC and C9DC in solid presented a narrow and sharp bands attributable to the ICT emissions at 550 nm and 565 nm, respectively. The intramolecular rotation was likely prohibited because of the steric hindrances of the substitutes in *o*-carborane units[23]. Moreover, the compounds are insensitive to the temperature due to their rigid structure, only enhanced emission intensity observed for all compounds rather than change the emission wavelength during cooling from 333 K to 77 K. From the above results, it can be concluded that *o*-carborane acts as a versatile "element-block" not only for constructing ICT emission but also for designing AIE luminogens with stronger fluorescence in solid.

To better understand the AIE characteristics and stronger fluorescence of C3DC and C9DC, the fluorescence lifetime was measured in various states and the radiative and nonradiative decay processes were also investigated (Fig 7 and Table 2). The radiative decay rate and nonradiative decay rate in solution compared to that of the rigid state, the radiative decay rate (k_{rad}) of C3DC increased by around 3 times ($k_{rad,solid}$=1.52×10^7 s^{-1} and $k_{rad,film}$=1.53×10^7 s^{-1}), while the nonradiative decay rate (k_{nr}) decreased almost by 300 times ($k_{nr,solid}$=0.15×10^5 s^{-1} and $k_{nr,film}$=0.13×10^5 s^{-1}). This suggests that the inhibition of nonradiative decay of excited state in the solid state is accounted for its high fluorescence. In sharp contrast, the k_{rad} of C3DC increased over 3 times than that of C9DC in the solid state, while k_{nr} decreased 20 times. In a word, the different reactive sites have a noticeable impact on photophysical properties of *o*-carborane containing carbazole derivative compounds.

Table 2 The photophysical properities of C3DC and C9DC in different states

Samples	State	τ_F/ns[e]	K_r/×10^{7}s^{-1}[f]	K_{nr}/×10^{7}s^{-1}[f]
C3DC	*Sol*[a]	2.91	-[g]	-[g]
	Agg[b]	9.81	0.58	0.44
	Solid[c]	6.58	1.52	0.001 5
	Film[d]	7.77	1.51	0.001 3
C9DC	*Sol*[a]	2.41	-[g]	-[g]
	Agg[b]	20.01	0.17	0.33
	Solid[c]	14.18	0.47	0.03
	Film[d]	13.88	0.62	0.10

Note: *a*: In THF; *b*: f_W= 99%; *c*: In the solid state; *d*: In neat film; *e*: λ_{ex}=340 nm; *f*: Fluorescence emission rate constant (k_r) and non-radiative decay rate constant (k_{nr}) were calculated as follows: $k_r=\Phi_f/\tau_f$, $k_{nr}=(1-\Phi_f)/\tau_f$; *g*: Not detected.

2.3 DFT Calculation

To ensure electronic alteration in functional carbazole groups driven by *o*-carborane, geometry optimization as well as the orbital contribution from HOMO and LUMO energies were performed on the B3LYP functional and 6-31 G (d, p) basis sets using Gaussian and the results are shown in Fig 8.

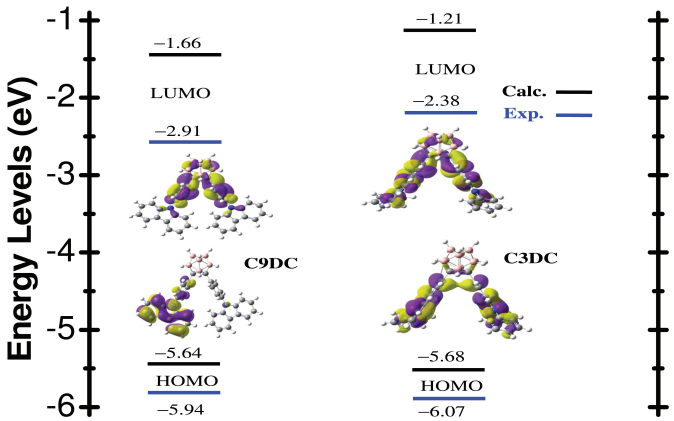

Fig 8 Frontier molecular orbitals and energy levels of HOMOs and LUMOs of C3DC and C9DC were calculated by DFT at B3LYP/6-31 G (d, p) level with Gaussian 09 W

The energy gap between HOMO and LUMO of C3DC and C9DC are 2.73 eV and 3.30 eV, respectively, and its energies changes concerning the reactive sites of carbazole groups with *o*-carborane. As expected, the electron cloud of HOMOs in C3DC mainly located in the carbazole groups and LUMOs on the C_{cage}–C_{cage} bond in *o*-carborane. LUMOs are mixed with carbazole groups and cage carbon orbitals and depending on the reactive sites of carbazole groups. However, for C9DC, the electron cloud of HOMOs mainly located in the carbazole groups, while the LUMOs lie on the entire molecules. LUMOs are mixed with carbazole groups and cage carbon orbitals and depending on the reactive sites of carbazole groups. This finding is another clear evidence for the difference electronic communication between carbazole and the *o*-carborane unit.

Table 3 The major low-energy electronic transitions for C3DC and C9DC in their ground state (S_0) and first excited singlet (S_1) states as calculated using TD-B3LYP with the 6-31 G (d,p) basis set[a]

Samples	State	λ_{calc}/nm	f_{calc}	Assignment
C3DC	S_0	318	0.036 1	HOMO→LUMO
	S_1	537	0.179 1	HOMO→LUMO
C9DC	S_0	357	0.113 8	HOMO→LUMO
	S_1	545	0.233 7	HOMO→LUMO

Note: *a*: Singlet energies for vertical transitions as calculated for the optimised S_1 geometries.

Time-dependent DFT (TD-DFT) calculations were performed according to the optimized geometries to locate the origin of the low energy absorptions of each type of carbazole groups (Fig 9). The low energy absorptions were attributed to the transitions from HOMO to LUMO, shifting from π (carbazole) to π^* (C_{cage}–C_{cage} bond) and transitions observed at λ_{max} as well as their relative energies and oscillator strength values are consistent with the UV-Vis absorption spectra (Fig 1 and Table 3). In addition, we optimized the excited state structures of C3DC and C9DC through TD-DFT calculations in the gas phase (Fig 9). It was revealed that the S_0–S_1 electronic transition was mainly derived from HOMO to LUMO. The HOMOs in C3DC and C9DC were localized on the π-conjugated carbazole moiety. In contrast, the LUMOs were significantly delocalized to the *o*-carborane moiety. This result also strongly supports that the emission should be derived from the CT states.

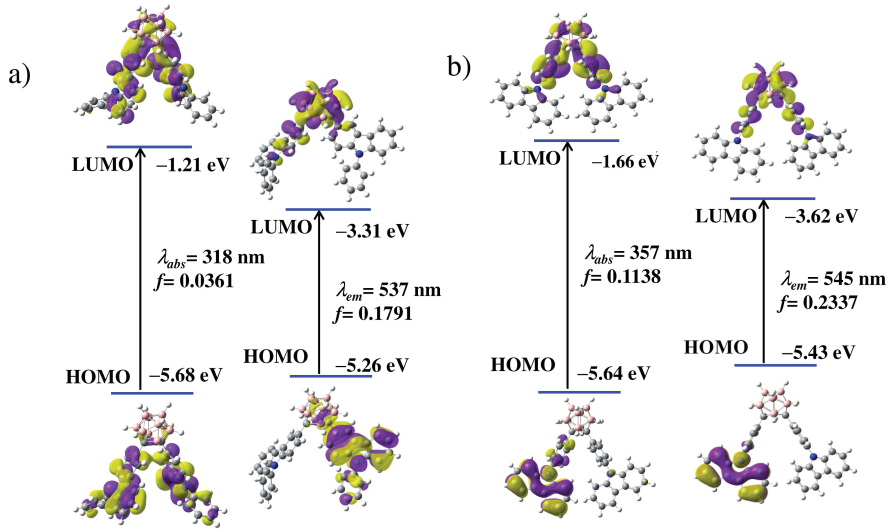

Fig 9 Frontier molecular orbitals of (a) C3DC and (b) C9DC in their ground state (S_0) and first excited singlet (S_1) states with relative energies calculated at the B3LYP/6-31 G (d, p) level of theory. The transition wavelengths (nm) were calculated at the TD-B3LYP/6-31 G (d, p) level of theory

3 Conclusion

We demonstrate that the introduction of skeletal distortion by *o*-carborane with regioisomeric N-phenyl-carbazole is a facile strategy for obtaining AIE-active molecules. From the comparison with regioisomeric N-phenyl-carbazole based *o*-carborane complexes, it was found that none of the *o*-carborane functionalized N-phenyl-carbazole compounds exhibited emission in the solution state at room temperature the emission peak intense location in the region of 540 nm~560 nm in

rigid states (i.e. in THF at 77 K, in solid and films state), and all demonstrated the enhanced ICT-based emission. The two *o*-carborane-functionalised N-phenyl-carbazole compounds have high solid-state fluorescence quantum yields, reaching 99% and 93%, respectively. DFT calculation results show that the intense emission bands attributable to ICT transitions from N-phenyl-carbazolemoieties to the *o*-carborane units. Consequently, the results of this study confirm the *o*-carborane attached to the different sites of the carbazole moiety can regulate the emission process based on ICT transitions.

References:

[1] OKSANA O. Organic optoelectronic materials: mechanisms and applications[J]. Chemical Reviews, 2016, 116(22): 13279-13412.

[2] HONG Y N, LAM W Y, TANG B Z. Aggregation-induced emission: phenomenon, mechanism and applications[J]. Chemical Communications, 2009, 29: 4332-4353.

[3] ROBERT C K, ALBERT F U, ORIOL C, et al. Ru(II) and Ir(III) phenanthroline-based photosensitisers bearing *o*-carborane: PDT agents with boron carriers for potential BNCT[J]. Biomaterials Science, 2021, 9(16): 5691-5702.

[4] WEE K R, CHO Y J, JEONG S, et al. Carborane-based optoelectronically active organic molecules: wide band gap host materials for blue phosphorescence[J]. Journal of the American Chemical Society, 2012, 134(43): 17982-17990.

[5] ZHANG M L, DING N N, LAI F Y, et al. Nonplanar perylene monoimide-based fluorescent film for enhanced BTX sensing[J]. Chinese Journal of Chemistry, 2021, 39(8): 2088-2094.

[6] LEE S H, MUN M S, LEE J H, et al. Impact of the electronic environment in carbazole-appended *o*-carboranyl compounds on the intramolecular-charge-transfer-based radiative decay efficiency[J]. Organometallics, 2021, 40(7): 959-967.

[7] KIM S, LEE J H, SO H, et al. Insights into the effects of substitution position on the photophysics of mono-*o*-carborane-substituted pyrenes[J]. Inorganic Chemistry Frontiers, 2020, 7(16): 2949-2959.

[8] OCHI J, TANAKA K, CHUJO Y. Recent progresses in the development of solid-state luminescent *o*-carboranes with stimuli responsivity[J]. Angewandte Chemie International Edition, 2020, 59(25): 9841-9855.

[9] WANG Z J, ZHAO J W, MUDDASSIR M, et al. Recovering the thermally activated delayed fluorescence in aggregation-induced emitters of carborane[J]. Inorganic Chemistry, 2021, 60(7): 4705-4716.

[10] WEE K R, HAN W S, CHO D W, et al. Carborane photochemistry triggered by aryl substitution: carborane-based dyads with phenyl carbazoles[J]. Angewandte Chemie International Edition, 2012, 51(11): 2677-2680.

[11] NAITO H, MORISAKI Y, CHUJO Y. *o*-Carborane-based anthracene: a variety of emission behaviors[J]. Angewandte Chemie International Edition, 2015, 127(17): 5173-5176.

[12] ZHOU Q, ZHU M, CHEN W, et al. Configuration-controllable synthesis of Z/E isomers based on *o*-carborane-functionalized tetraphenylethene[J]. New Journal of Chemistry, 2021, 45(29): 12830-12837.

[13] WU X Y, GUO J X, ZHAO J Z, et al. Multifunctional luminescent molecules of *o*-carborane-pyrene dyad/triad: flexible synthesis and study of the photophysical properties[J]. Dyes Pigments, 2018, 154: 44-51.

[14] MARSH A V, CHEETHAM N J, LITTLE M, et al. Carborane-induced excimer emission of severely twisted bis-*o*-carboranyl chrysene[J]. Angewandte Chemie International Edition, 2018, 57(33): 10640-10645.

[15] WU X Y, GUO J X, LYU Y, et al. Aggregation-induced emission characteristics of *o*-carborane-functionalized fluorene and its heteroanalogs: the influence of heteroatoms on photoluminescence[J]. Materials Chemistry Frontiers, 2020, 4(1): 257-267.

[16] WU X Y, GUO J X, CAO Y L, et al. Mechanically triggered reversible stepwise tricolor switching and thermochromism of anthracene-*o*-carborane dyad[J]. Chemical Science, 2018, 9(23): 5270-5277.

[17] FRISCH M J, TRUCKS G W, SCHLEGEL H B, et al. Gaussian 09 W(Revision B.01)[M]. Wallingford: Gaussian Inc, 2010.

[18] LI J L, GRIMSDALE A C. Carbazole-based polymers for organic photovoltaic devices[J]. Chemical Society Reviews, 2010, 39(7): 2399-2410.

[19] CHEN Y, GUO J X, WU X Y, et al. Color-tuning aggregation-induced emission of *o*-carboranebis(1,3,5-triaryl-2-pyrazoline) triads: preparation and investigation of the photophysics[J]. Dyes Pigments, 2018, 148: 180-188.

[20] JIN G F, CHO Y J, WEE K R, et al. BODIPY functionalized *o*-carborane dyads for low-energy photosensitization[J]. Dalton Transactions, 2015, 44(6): 2780-2787.

[21] WU X Y, GUO J X, QUAN Y J, et al. Cage carbon-substitute does matter for aggregation-induced emission features of *o*-carborane-functionalized anthracene triads[J]. Journal of Materials Chemistry C, 2018, 6(15): 4140-4149.

[22] KOKADO K, CHUJO Y. Multicolor tuning of aggregation-induced emission through substituent variation of diphenyl-*o*-carborane[J]. The Journal of Organic Chemistry, 2011, 76(1): 316-319.

[23] NATIOH, NISHINO K, MORISAKI Y, et al. Solid-state emission of the anthracene-*o*-carborane dyad from the twisted-intramolecular charge transfer in the crystalline state[J]. Angewandte Chemie International Edition, 2017, 56(1): 254-259.

责任编辑：艾合麦提·吾买尔